Physical characterization of nanoimprinted polymer nanostructures using visible light angular scatterometry

Rayan M. Al-Assaad
Li Tao
Wenchuang Hu
University of Texas at Dallas
Nanoscale Integration Laboratory
Department of Electrical Engineering
Erik Jonsson School of Engineering and Computer Science
Richardson, Texas 75083
E-mail: walter.hu@utdallas.edu

Abstract. Visible light angular scatterometry is applied to characterize the geometry and physical properties of sub-100-nm-wide polymer gratings fabricated using nanoimprint lithography and electron beam lithography. Measurement sensitivities to small variations in linewidth and slope angle were evaluated theoretically, which suggests that TM polarized incident light offers improved sensitivity for the measurements of sub-45-nm critical dimensions (CDs). A variable angle scatterometer using a red laser is built, and measurement results of various polymethylmethacrylate (PMMA) gratings with sub-100-nm CDs reveals good accuracies and fit well to the scanning electron microscopy (SEM) measurements. In addition to geometry and dimension measurements, new functionality is implemented in the modeling to characterize polymer residue thickness, polymer flow dynamics, and evidence of stress in the nanoimprinted polymer gratings. Scatterometry is also applied to detect possible undercut line profiles resulting from electron beam lithography. The results promote using this low-cost and noninvasive technique to characterize polymer nanostructures as well as understand and control the underlying lithographic processes. *© 2008 Society of Photo-Optical Instrumentation Engineers.* [DOI: 10.1117/1.2894772]

Subject terms: scatterometry; critical dimension (CD) metrology; nanoimprint lithography; electron beam lithography; polymer; nanostructures.

Paper 07024 received Mar. 3, 2007; accepted for publication Sep. 24, 2007; published online Mar. 18, 2008.

1 Introduction

The ability to fabricate polymeric nanostructures is of fundamental importance for the evolution of integrated circuit (IC) technology and many emerging optical, electromechanical, and biomedical nanodevices and systems. For IC fabrication, polymer nanopatterns are formed with photolithography and then used as masks to transfer lithographic patterns into solid state materials. However, with the recent advancement of polymer chemistry, polymer nanostructures are becoming popular device components that can bring more functionality and performance with lower cost. For the fabrication of polymer nanostructures, nanoimprint lithography (NIL)[1] excels as a cost-effective manufacturing technique with resolution smaller than 5 nm.[2,3] The UV version of NIL including step and flash imprint lithography (S-FIL)[4] has already been considered by the semiconductor industry since 2004 as a candidate for the next-generation lithography technology.[5]

With down-scaling of patterning resolution, metrology becomes increasingly challenging. The semiconductor industry has already set stringent requirements for critical dimension (CD) metrology for the 45-nm node and beyond.[5] The combination of CD-SEM (scanning electron microscopy), CD-AFM (atomic force microscopy), and scatterometry is expected to continuously improve for the quickly approaching nano-era.[6] However, for nanoimprinted polymer nanostructures as permanent device components, CD-SEM becomes destructive, and AFM cannot measure residue thickness and suffers from resolution limitation due to the tip effect. In addition, there is a need to characterize residue thickness, stability, and internal stress of imprinted polymer nanostructures in order to control nanoimprint processes to achieve good fidelity. Recently, nondestructive and highly sensitive techniques based on small-angle x-ray scattering (CD-SAXS)[7,8] and specular x-ray reflectivity (SXR) from periodic patterns have been developed at NIST to characterize polymeric grating dimensions and to monitor the real-time evolution of polymer nanostructures during thermal annealing.[9] However, the wide spread of CD-SAXS may be limited by the high cost of strong x-ray sources as well as x-ray invasive radiations in functional polymers.

We have explored the feasibility of using variable-angle scatterometry with visible wavelengths as a high-precision, low-cost, and noninvasive metrology for characterizing dimensions, profile geometry, residue thickness, and polymer flow behaviors of nanoscale polymer gratings. Scatterometry[10] has been explored extensively for semiconductor submicrometer and nanometer dimensional metrology. The technique refers to the measurements of reflected power upon the interaction of an incident beam with some periodic surface (grating). The characteristics of the diffractive surface directly affect the acquired measurements. Therefore, it is possible to resolve some information about the grating line profile and dimensions from the mea-

1537-1646/2008/$25.00 © 2008 SPIE

surements, which is sometimes referred to as the inverse scatterometry problem. Previously, spectral scatterometry has been applied to measure the residue thickness of imprinted microscale and sub-μm patterns.[11] Other assessment shows that spectral scatterometry faces increasing challenges, such as decreasing sensitivity with CDs <20 nm (Ref. 6).

In contrast to spectral scatterometry, the visible light angular scatterometry (VLAS) that we propose here shows promising sensitivity with CD down-scaling. In VLAS, the pitch of nanoscale patterns is significantly smaller than the wavelength, and therefore reflected light undergoes no or very little diffraction from the periodic surface. Using computer simulations, both TE and TM polarized light were investigated where the electric field oscillates parallel or normal to the grating lines, respectively. Gratings with 65-nm, 45-nm, 32-nm, and 22-nm CDs were examined that represent current and future semiconductor technology nodes. For such dimensions, the sensitivities in the reflectance measurements to the small changes in the line profiles (width and slope) are assessed based on the rigorous coupled wave approximation (RCWA).[12] The theoretical studies reveal good sensitivity and sufficient accuracy in CD detection down to 20 nm using visible wavelengths. In fact, it is shown that when the grating dimensions decrease, the sensitivities could be increased in some situations.

The theoretical findings are then followed up with experimental studies based on two-dimensional (2-D) gratings with sub-100-nm poly(methylmethacrylate) (PMMA) lines fabricated using both NIL and e-beam lithography (EBL). The experimental data were acquired with an in-house angular scatterometry setting. The line profile geometries were resolved using a linear regression solution model that has been established previously[8] based on the RCWA. Trapezoid line profile models are used in scatterometry to find average grating height, top width, and sidewall slope angle. In order to characterize the residue thickness and also polymer flow behaviors for NIL processes, a more complicated model that takes into account the residue layer and nonlinear sidewalls has been developed. Nanoimprinted samples with different initial thickness were investigated. The residue layer thickness and line geometry were well resolved, uncovering a noticeable effect of PMMA thickness on the resulting profile geometry. We also demonstrate applying VLAS to study polymer flow behavior. An imprint sample was characterized before and after heating, revealing high fidelity in retrieving the nonlinear line profile due to "melting." The profile evolution observed provides evidence of nonuniform distribution of imprint-induced stress in polymer nanostructures. Physical characterization of polymer nanostructures generated by EBL is also investigated. The VLAS results of both NIL and EBL were in good agreement with the SEM profile images. These results show the feasibility of this low-cost metrology tool in resolving physical information about nanostructures with high accuracy.

2 Scatterometry Setup and Sensitivities Analysis

2.1 *Scatterometry Setup*

To investigate the feasibility of using visible light metrology for the characterization of sub-100-nm line profiles and

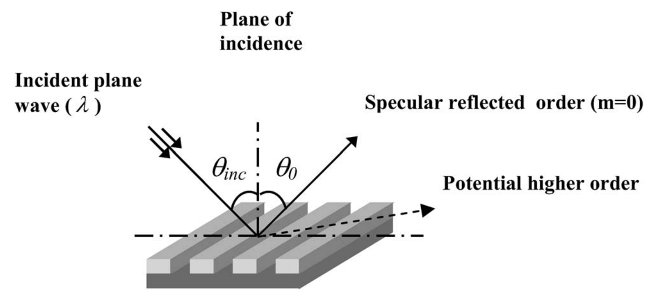

Fig. 1 Schematics of a 2-θ angular scatterometry configuration.

dimensions, a variable angle scatterometer is built based on a 2-θ configuration (Fig. 1) using a red laser, a linear polarizer, a chopper, and three lenses to focus the beam onto the center of the grating sample. The incident beam and the normal to the diffracting surface form the plane of incidence, which is usually perpendicular to the directions of the grating. The direction of propagation of all reflected diffracted orders (designated by angle θ_m) is given by the grating equation,

$$\sin\theta_{inc} + \sin\theta_m = \frac{m\lambda}{a}, \tag{1}$$

where the angles θ_{inc} and θ_m correspond, respectively, to the incident and the m'th order reflected beams measured relative to the normal to the grating surface in the plane of incidence, λ is the wavelength of the incident beam, a is the pitch of the grating, and m is an integer that designates the specific diffracted order ($m=0,\pm1,\pm2,\ldots$). When the incident beam is linearly polarized such that the electric field strength oscillates perpendicular to the plane of incidence and parallel to the grooves of the diffracting structure, the polarization state is referred to as TE or s. The polarization state orthogonal to TE is known as TM or p, where the electric field strength oscillates parallel to the plane of incidence and perpendicular to the gratings. The instrument is fixed to operate in the TM mode for all the measurements in this paper for better sensitivity, as discussed in the next section. It is common, although not necessary, to measure only the specular order ($m=0$). The resulting grating equation reduces to $\theta_0=-\theta_{inc}$. In the angular configuration, measurements are made by varying the angle of incidence over a chosen range and recording the reflected zeroth (specular) order power at each corresponding angle of reflectance, maintaining a constant wavelength. The diameter of the focused beam spot is measured using a beam profiler tool and is estimated below 20 μm at normal incidence. The angular measurements are acquired by rotating the sample stage with a motor connected to a standard PC and controlled by software. The reflectance measurements are collected for the zeroth order using an Si photodiode.

2.2 *Sensitivities to Small Width and Sidewall Slope Variations*

Attempts based on angular or spectral ellipsometry have been made previously to improve the capability of scatterometry in resolving sub-100-nm dimensions.[13,14] Measure-

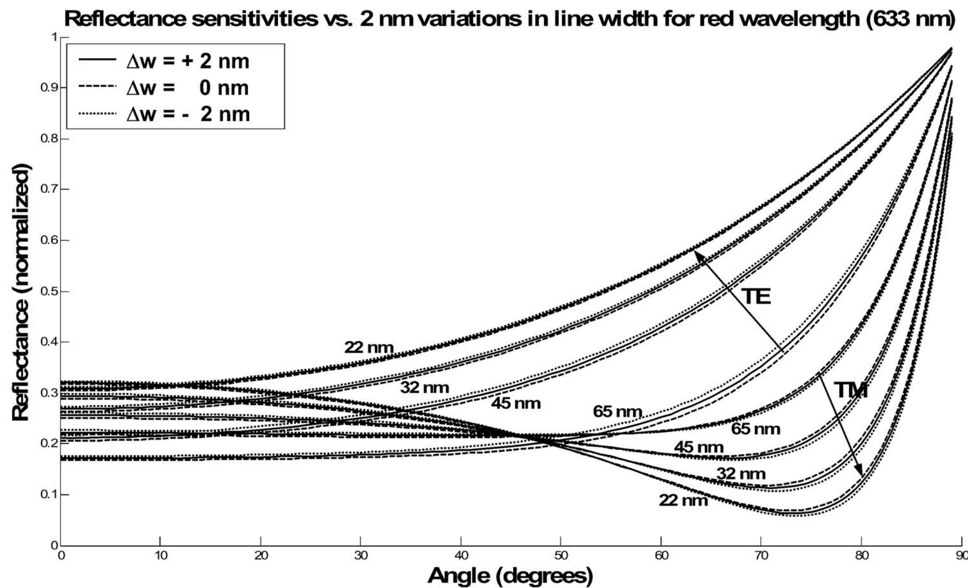

Fig. 2 Simulated TM and TE angular reflectance measurements ($\lambda = 633$ nm) for four different rectangular profile gratings (PMMA on Si). The gratings periods are specified at 130 nm, 90 nm, 64 nm, and 44 nm with linewidths of 65 nm, 45 nm, 32 nm, and 22 nm, respectively. For all grating profiles, the height value is set equal to twice the width value to maintain a constant line aspect ratio. For each set, the sensitivities in the reflectance curves are shown for 2-nm variations in the width values (Δw). The measurement sensitivities for smaller line pitch and width values are found to be higher in the TM reflectance mode and smaller in the TE mode.

ment sensitivities using visible wavelength angular scatterometry have also been investigated theoretically, anticipating limitations of this approach.[15] Here, we reexamine the red wavelength (633 nm) measurement behavior for sub-100-nm CD with both the TE and TM polarization modes, using the RCWA model in order to uncover some conditions to further improve the sensitivities. PMMA gratings on Si with rectangular profiles are considered with widths of 65 nm, 45 nm, 32 nm, and 22 nm; 1:1 line-to-space ratio; and 2:1 height-to-width ratio. For each of the four CDs, a set of three simulated reflectance curves is generated that correspond to 2-nm changes in the width for both TE and TM modes, as shown in Fig. 2. This shows that in the case of TE polarization, the measurement sensitivities to 2-nm-width variations decrease as the profile dimensions and pitch decrease, while for the TM case, the sensitivities increase. The increased sensitivity is especially noticeable around the angles with minimum TM reflectance values.

In an experimental situation with additive random noise characteristics, the mean noise-to-signal ratio is defined usually as the average ratio of error in reflectance values to the actual reflectance values across the range of angles considered. The mean noise-to-signal ratio across all angles is expected to be smaller than 1% in a well-controlled instrument setting. In order to obtain a sensitivity measure that can be weighed against the mean noise-to-signal ratio, the mean in reflectance differences (due to small width variations) to reflectance values, i.e., $(\overline{\Delta R}/\bar{R}) \times 100$, is chosen, where $\overline{\Delta R}$ is the average reflectance difference, and $\bar{R}$ is the average reflectance value for all angles considered. The measure of sensitivity $(\overline{\Delta R}/\bar{R}) \times 100$ is found greater than twice the required 1% mean noise-to-signal ratio in the TE but not the TM case for the 65-nm CD. In contrast, the value of $(\overline{\Delta R}/\bar{R}) \times 100$ is found greater than twice the 1% mean noise-to-signal ratio in the TM and not the TE case for the 22-nm CD. This again confirms the observation made in Fig. 2, where an increase in sensitivities is found in the TM mode as the line dimensions and pitch decrease. The sensitivity analysis therefore promises acceptable accuracy (down to 2 nm) in resolving the 20-nm CD using TM mode and red wavelength reflectance measurements. A similar study of measurement sensitivities for small variations in the sidewall slope parameter was also performed for both the TE and TM modes with the red incident wavelength. As shown in Fig. 3, each of the additional simulated sets consists of two reflectance curves that correspond to 0-deg sidewall slope (rectangle profile) and 5-deg sidewall slope (trapezoid profile). The reflectance sensitivities for the TM mode are found comparable for all CD sizes and slightly decrease for the TE mode as the line CD decreases. In comparison to the width variation study, the sensitivities appear larger here for all CDs. These theoretical findings for the subwavelength gratings are encouraging and show good potential for visible light angular measurements in resolving sub-45-nm CDs. In the next section, experimental results based on the VLAS setting in the TM mode and using a red light source are presented.

3 Experimental Procedure

3.1 *Fabrication of Polymer Gratings*

PMMA with 950 K molecular weight was spincoated onto Si substrates with varying thicknesses from 220 nm to 620 nm, as measured by spectral ellipsometer as well as profilometry. An Si mold was used to generate sub-100-nm gratings on both 220-nm and 620-nm PMMA films

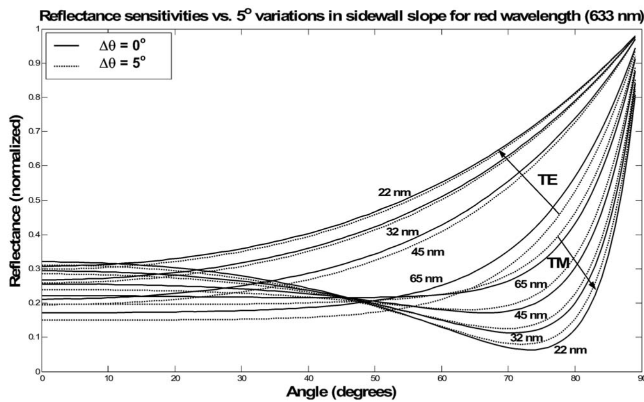

Fig. 3 Simulated TM and TE data sets (λ=633 nm) for the four gratings in Fig. 2. For each set, two reflectance measurements are shown to reflect the measurement sensitivities to 5 deg change in the sidewall sloe angle ($\Delta\theta$). The measurement sensitivities are found to be similar in the TM reflectance mode and smaller in the TE mode as line pitch and width values decrease.

using an Obducat 2.5 nanoimprinter at a temperature of 180 °C (~80° above Tg of PMMA) and a pressure of 6 MPa for 10 min. The mold was released from the PMMA substrates after cooling to below Tg of PMMA. The PMMA patterns cover an area of 2×4 mm^2 consisting of periodic groups of 9-μm-long nanogratings in one direction separated by 1-μm-wide gaps perpendicularly, as shown in Fig. 4.

In comparison with the imprinted polymer nanostructures, EBL was used to fabricate similar gratings with ~50-nm width in 250-nm-thick PMMA on Si substrates using a Zaiss Supra 40 field emission SEM with a NPGS 9.2 pattern generator. Due to limitations in the e-beam machine regarding the extent of writing area and exposure time, a 1×1 mm^2 2-D grating array with large gaps was made instead of a large array of continuous lines, in a manner similar to nanoimprinted patterns, as shown in Fig. 5. For this sample, the gap pitch, line length, and line pitch were specified at 20 μm, 5 μm, and 200 nm, respectively. After EBL, the sample was developed in methyl isobutyl ketone: isopropyl alcohol (1:3) for 1 min.

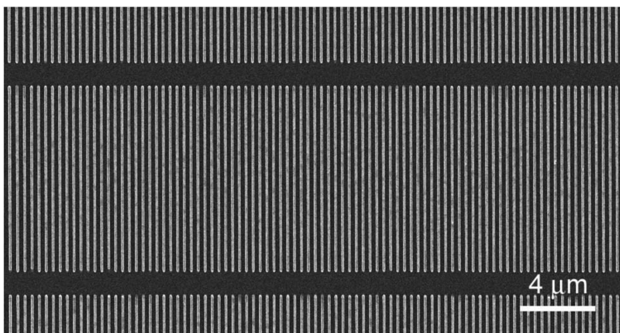

Fig. 4 An SEM top view of the 2-D array nanoimprinted PMMA gratings. The line length and pitch in the parallel direction are estimated at 9 μm and 10 μm, respectively. The smaller pitch perpendicular to the line direction is estimated at 365 nm.

3.2 *Scatterometry Measurements*

The polymer samples were measured using the VLAS setup by varying the angle of incidence from 20 deg to 80 deg and measuring only the zeroth-order reflected intensity for each angle. A linear regression algorithm[16] is used to process the angular reflectance data and retrieve the line profile in addition to the residue thickness by fitting the measurements to the RCWA model. A trapezoid model is chosen for the line profile, characterized using three geometric parameters: height, width, and sidewall slope angle. This model is feasible for EBL samples. However, for nanoimprinted gratings, there is a residue layer formed underneath the gratings, and in addition, imprinting under high pressure could increase the polymer density of the gratings. Therefore, the residue thickness and PMMA index were also optimized in addition to the three profile geometric parameters to characterize nanoimprinted samples. The refractive index values of the initial PMMA films were obtained using ellipsometry. After the scatterometry data were collected, these PMMA grating samples were sputter-coated with a few-nanometers-thick AuPd (60:40) and cleaved for cross-sectional SEM imaging. Then the scatterometry measurement results and SEM images were compared.

In addition to scatterometry measurements, the pitch of the gratings is first estimated using the 2-θ setup. This is achieved by locating the incident angle where the +first reflected order begins propagating using a red HeNe laser beam (633-nm wavelength). From the grating equation relationship, the period is then readily calculated once the wavelength and the incident cutoff angle for the first order are known, as follows:

$$a=\frac{\lambda}{1+\sin\theta_{inc}}, \tag{2}$$

where a is the grating pitch, λ is the beam wavelength, and θ_{inc} is the incident cutoff angle. According to this formula, the grating pitch is calculated at 365 nm for the imprinted samples and 200 nm for the EBL samples. The pitch values and line length estimates matched well the SEM measurements. For this kind of 2-D pattern, the reflectance values are most sensitive to the grating dimensions, followed by the grating pitch, and are least sensitive to the large grating length or gap pitch (10 μm for the imprinted sample, and 20 μm for the EBL samples). For this reason, some degree of estimation error is tolerated for the large pitch and line length values. The grating pitch value is also estimated with an uncertainty error range of few nanometers that is negligible with respect to the red measurement wavelength used.

4 Results and Discussion

4.1 *Scatterometry on Nanoimprinted Polymer Gratings*

Reflectance data and scatterometry results for the imprinted gratings on the 220-nm and 620-nm PMMA films are shown in Fig. 6(a). The sum square error (sse) in the optimized data (reflectance curves) is smaller in the case of the thin PMMA sample. The larger sse error in the case of the thick PMMA sample may be caused by a nonuniform residue layer, which might result from the mold bending on the thick PMMA during imprinting. The sample cross sections

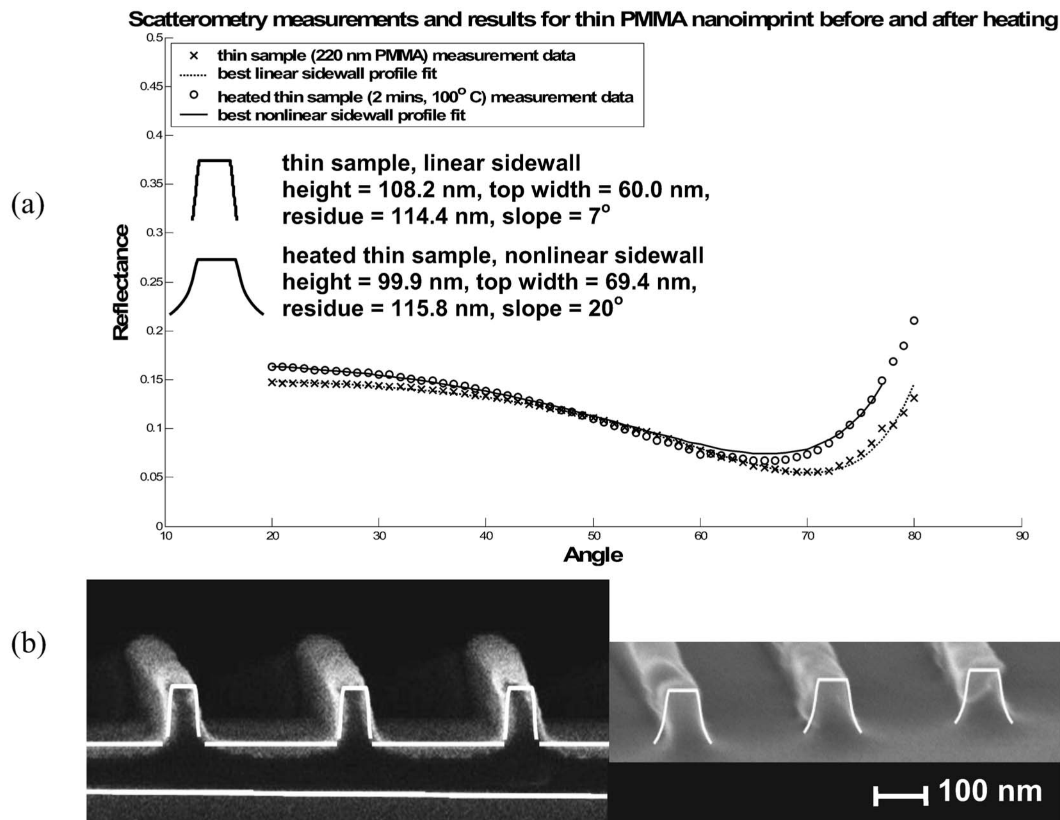

Fig. 5 (a) Reflectance measurements and modeling results for the thin PMMA nanoimprint sample before and after heating at 100 °C for 2 min. The nonlinear sidewall profile model shows a good fit with the (b) grating profile in the SEM cross-sectional images. A reduction of 8.3 nm to the grating height and an addition of 9.4 nm to the linewidth were measured. The sidewall slope was found to increase from 7 deg to 20 deg and to exhibit stronger nonlinearity after heating. The residue layer has not changed significantly due to a short annealing time.

were evaluated in SEM, and a 40-nm variation of residue layer thickness was observed across a 2-mm pattern area. The gratings on the thicker PMMA sample are measured to be 126.0-nm tall and 80.7-nm wide at the top, with a 0.3-deg slope angle and a residue layer of 349.5 nm. The gratings on the thinner sample are measured and found to be 108.2-nm tall and 60.0-nm wide with a 7-deg slope angle and a residue layer of 114.4 nm. The results were also compared to the SEM images in Fig. 6(b), revealing good accuracies. Using the error covariance matrix established in previous work,[17] the errors in the reported residue, height, and width parameters are found around 1-nm, 2-nm, and 4-nm uncertainty range, respectively, based on an estimated measurement noise level at 0.05%. The uncertainty error range is an indication of the measurement sensitivity to small changes in a parameter. The largest uncertainty error in the reported width parameter hence reveals the least measurement sensitivities. It is expected that uncertainty errors for the width parameter will be further reduced as the sample pitch decreases and measurement sensitivities increase, based on the sensitivity analysis presented earlier.

The scatterometry results along with the SEM images indicate that under the same NIL conditions, different initial PMMA thicknesses have resulted in variation of polymer filling into the mold. Thicker PMMA film would result in more complete filling than the thinner one. As a result, gratings formed on the thicker PMMA appear 17.8 nm (16.5%) taller with a smaller sidewall slope and 20 nm (33.3%) wider on the top than the thinner sample. These results suggest that the residue thickness should be considered and optimized for the development of high-fidelity nanoimprint processes.

It is worth noticing that during the scatterometry modeling process, adding the PMMA index as a fifth parameter instead of using a constant value is found to enhance the optimization and yields more accurate results. According to previous simulated studies of polymer flow during NIL, the resulting average PMMA density is expected to be higher for molds with smaller linewidth and initial polymer film thickness.[18] However, there is no experimental evidence reported yet, due to the difficulty of index measurement on these nanostructures. In our scatterometry results in Fig. 7, an average PMMA index was found unchanged at 1.48 for the thick sample but found to increase to 1.9 in the thin sample after the imprint process. However, more samples with various line dimensions and residue thickness should be measured before arriving at a conclusive understanding on the relation between resist thickness and polymer density distribution after imprinting.

Besides the characterization of the three-dimensional (3-D) geometry and residue thickness, VLAS was used to monitor shape evolution of polymer nanostructures during thermal annealing, which relates to important polymer stability issues. Here, a nonlinear sidewall model is used to

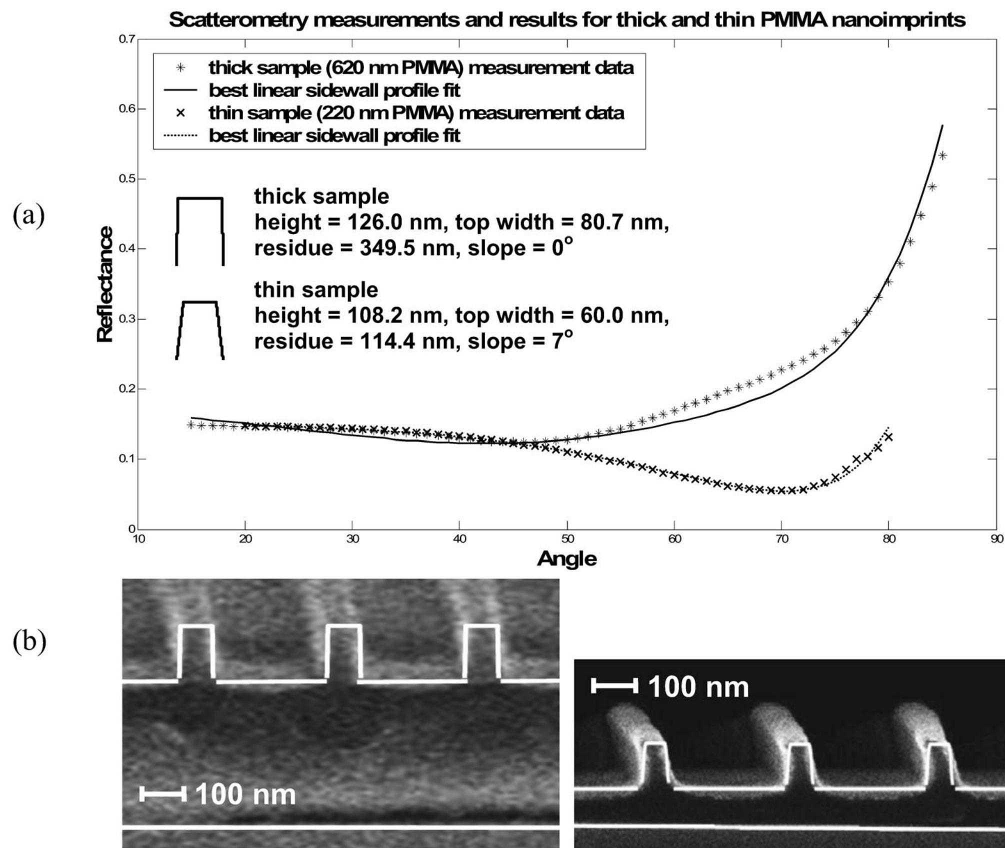

Fig. 6 (a) Reflectance measurements and modeling results for 620-nm and 220-nm PMMA nanoimprinted samples from the same mold. The resolved profiles (white lines over SEM images) show a good fit with the (b) grating profiles in the SEM cross-section images. The thin PMMA sample appears to be shorter and with a more slanted sidewall. The residue layer in both cases is estimated with good accuracy. For the thick sample, the larger difference between the model reflectance curve and the data suggests a nonuniform residue layer. This problem does not arise when a thin PMMA layer is used. The data indicate that the scatterometry offers high sensitivity to detect the thickness of the polymer residue layer as well as grating dimensions and line profile.

reveal more faithful representation and insight over the polymer flow behavior. The nonlinear sidewall is implemented using finite layers of rectangles with varying width in the RCWA-based model. A larger number of layers will offer more precise representation of the profile but increase computation time significantly. As a trade-off, a 10-layer model was used. Figure 5(a) shows the scatterometry results of the PMMA gratings imprinted on the 220-nm PMMA films before and after a thermal annealing for 2 min at 100 °C, which is slightly above the Tg of PMMA (95 °C). Two SEM images of grating cross sections before and after annealing are shown in Fig. 5(b), indicating good accuracy of scatterometry measurements of the geometry as well as nonlinear profile slope. These scatterometry results show that after the short annealing, a more pronounced nonlinear sidewall profile was found, with only a slight change in height (reduction of 8.3 nm or 7.7%), top linewidth (increment of 9.4 nm or 15.7%), and residue thickness (1.4 nm or 1.2%). The average slope angle increased significantly from 7 deg to 20 deg. These results indicate that during thermal annealing, the polymer nanostructures seem to relax or expand most significantly at the bottom corners of the gratings, where high internal stress or high PMMA density is induced by the nanoimprint process, as predicted by the simulations in Ref. 18. Such instability behavior may also depend on residue thickness and polymer-substrate interaction. It is shown that this scatterometry setup along with the nonlinear sidewall model is a feasible characterization tool to study this phenomenon. A systematic study of the stability of polymer nanostructures on different residue thicknesses and longer annealing times using this method should reveal more insightful understanding in future work.

4.2 *Scatterometry on E-Beam Lithography Sample*

In comparison to NIL, similar PMMA gratings created using EBL were also studied using the same scatterometry setup. These PMMA gratings have uniform density and no residue layer. Reflectance data, scatterometry modeling, and cross-sectional SEM images for these gratings are shown in Fig. 7. Since PMMA is a positive resist and e-beam exposure created trenches in the PMMA film, a three-parameter trapezoid model is used for the trenches instead and a very good fit is obtained to the experimental data. The results reveal a rectangular profile with 0-deg sidewall slope angle and 48.7-nm trench width. An SEM image of the trench profile is compared to the scatterometry results, revealing an excellent match. The uncertainty errors in the reported height and width parameters are found around 1 nm and 2 nm, respectively. The improvement in

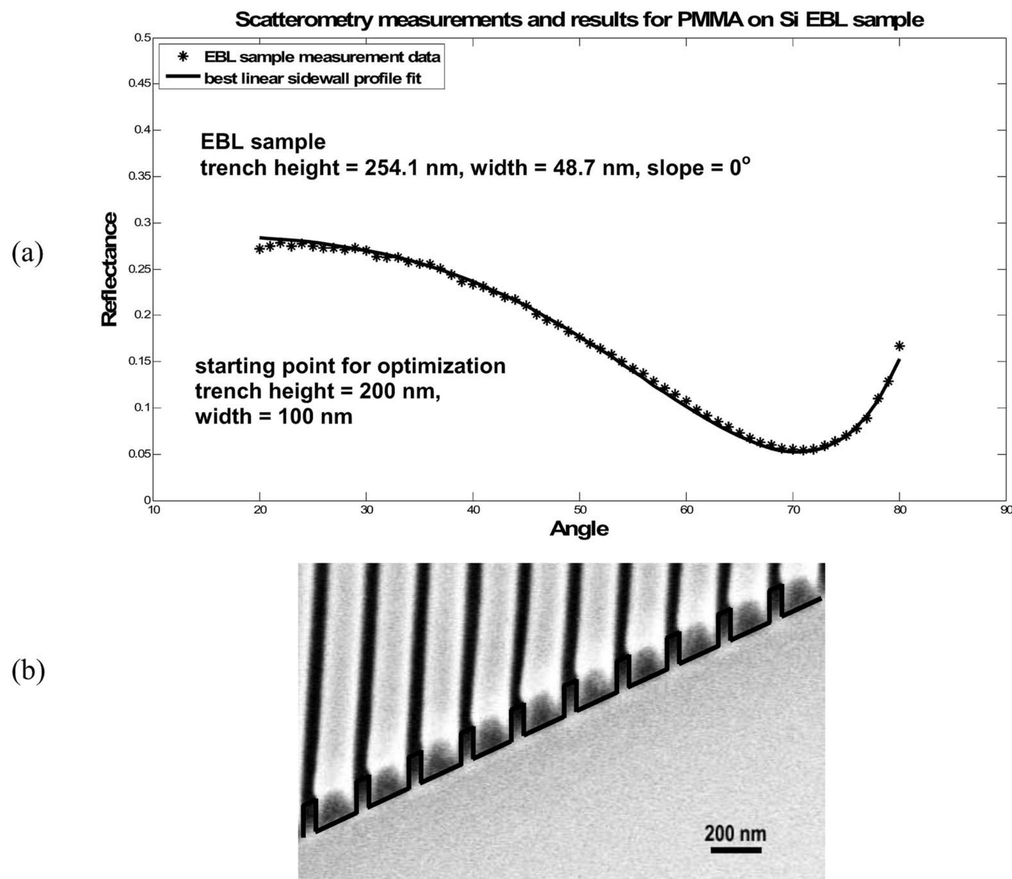

Fig. 7 (a) Reflectance measurements and modeling results for the EBL sample. The resolved trench profile is rectangular, revealing a minimal e-beam spread effect during exposure. Scatterometry results are in good agreement with (b) SEM cross-section images. Note: The EBL sample was cleaved at an angle of 30 deg with respect to the grating direction; hence a skewed SEM image of the trench profile is shown in the figure.

parameter estimation accuracy in the EBL sample in comparison to that in the imprint samples confirms the observations made in the sensitivity analysis mentioned earlier. The TM angular measurements are more sensitive to slight height and width variations in the smaller pitch EBL sample. This scatterometry technique shows the capability to characterize profile shapes of PMMA nanoscale trenches generated by EBL and can be used to reveal any undercuts without damaging the resist or cleaving the sample for SEM imaging.

5 Summary

Visible light angular scatterometry is applied to characterize the geometry and stability of polymer nanostructures fabricated by nanoimprint and e-beam lithography. A measurement sensitivity analysis is presented using RCWA for gratings with 65-nm, 45-nm, 32-nm, and 22-nm CDs. Both the TM and TE cases are analyzed. The measurement sensitivities are found to increase in the TM reflectance as the line features and pitch decrease. VLAS with TM incidence shows promising sensitivity to revolve 20-nm features. An angular scatterometry tool is built based on 2-θ configuration, and experimental measurements are performed for sub-100-nm PMMA gratings generated with NIL and EBL. For nanoimprinted gratings, in addition to the 3-D parameters describing the trapezoid profile geometry, the unknown PMMA residue layer and the average refractive index value after imprinting were also characterized. These scatterometry results fit well the SEM cross-sectional images of PMMA gratings and show good measurement accuracy at nanoscale. The measurements of PMMA gratings on two different residue thicknesses (349.5 nm and 114.4 nm) show that thicker initial film thickness results in better completed polymer filling into the mold during nanoimprinting owing to a larger PMMA reservoir in comparison to the thin sample. In addition, the average PMMA refractive index value was found to increase in the case of the thin PMMA sample, which provides evidence of stress in the nanostructures induced by imprinting. Moreover, a model based on multiple layers of rectangles is developed to characterize the nonlinear sidewall slope of PMMA gratings. With this model, the profile evolution of PMMA nanostructures during thermal annealing around the Tg temperature is characterized. These results provide evidence of polymer flow behaviors. Polymer nanostructures expand or relax most significantly at the high stress areas—in other words, the relaxation process during thermal annealing behaves like the reversal process of imprinting. For nanogratings created by EBL, a simple trapezoid model was used in scatterometry, and the measurement results are found in good agreement with SEM images for sub-50-nm trenches with 200-nm pitch in PMMA. VLAS shows the capability

of measuring an undercut line profile generated by EBL, which is an important control factor for the consequent lift-off process of EBL.

Based on these studies, we believe that with optimized measurement conditions and suitable models, the VLAS technique is a feasible metrology tool to characterize dimensions, geometry, residue thickness, as well as instability behaviors of polymeric nanostructures by nanoimprint and e-beam lithography. These measurements are rapid, highly accurate, low-cost, and noninvasive. Since both NIL and EBL play important roles in research, prototyping, and manufacturing of future nanodevices, the characterization of the geometry and behaviors of polymer nanostructures may provide insightful understanding and better control of underlying lithography processes.

Acknowledgments

We thank Dr. Dale M. Byrne at the University of Texas at Dallas for his in-kind donation of the parts for scatterometry and previous work on the equipment and also modeling algorithms. We also thank Prof. Stella W. Pang at the University of Michigan for her support on the mold fabrication. This work is supported in part by the Texas Higher Education Coordinating Board through the Advanced Research Program under Contract No. 009741-0015-2006. R. M. A. acknowledges support from the Eric Jonsson School of Engineering and Computer Science of the University of Texas at Dallas for a postdoctoral fellowship.

References

1. S. Y. Chou, P. R. Krauss, W. Zhang, L. Guo, and L. Zhuang, "Sub-10 nm imprint lithography and applications," *J. Vac. Sci. Technol. B* **15**(6), 2897–2904 (1997).
2. F. Hua, Y. Sun, A. Gaur, M. A. Meitl, L. Bilhaut et al., "Polymer imprint lithography with molecular-scale resolution," *Nano Lett.* **4**(12), 2467–2471 (2004).
3. M. D. Austin, H. X. Ge, W. Wu, M. T. Li, Z. N. Yu, D. Wasserman, S. A. Lyon, and S. Y. Chou, "Fabrication of 5 nm linewidth and 14 nm pitch features by nanoimprint lithography," *Appl. Phys. Lett.* **84**(26), 5299–5301 (2004).
4. D. J. Resnick, S. V. Sreenivasan, and C. G. Willson, "Step and flash imprint lithography," *Mater. Today* **8**(2), 34–42 (2005).
5. "2006 international technology roadmap for semiconductors," http://www.itrs.net/Links/2006Update/2006UpdateFinal.htm.
6. B. J. Rice, H. Cao, M. Grumski, and J. Roberts, "The limits of CD metrology," *Microelectron. Eng.* **83**(4–9), 1023–1029 (2006).
7. R. L. Jones, T. Hu, E. K. Lin, and W. Wu, "Small x-ray scattering for sub-100 nm pattern characterization," *Appl. Phys. Lett.* **83**(19), 4059–4061 (2003).
8. R. Jones, T. J. Hu, C. L. Soles, E. K. Lin, W. Hu, R. M. Reano, S. W. Pang, and D. M. Casa, "Pattern fidelity in nanoimprinted films using critical dimension small angle x-ray scattering," *J. Microlithogr., Microfabr., Microsyst.* **5**(1), 013001 (2006).
9. H. W. Ro, Y. F. Ding, H. J. Lee et al., "Evidence for internal stresses induced by nanoimprint lithography," *J. Vac. Sci. Technol. B* **24**(6), 2973–2978 (2006).
10. S. S. H. Naqvi, J. R. McNeil, R. H. Krukar, and K. P. Bishop, "Scatterometry and the simulation of diffraction-based metrology," *Microlithogr. World* **2**(3), 5–16 (1993).
11. D. Fuard, C. Perret, V. Farys, C. Gourgon, and P. Schiavone, "Measurement of residual thickness using scatterometry," *J. Vac. Sci. Technol. B* **23**(6), 3069–3074 (2005).
12. M. G. Moharam and T. K. Gaylord, "Rigorous coupled-wave analysis of planar-grating diffraction," *J. Opt. Soc. Am.* **71**(7), 811–818 (1981).
13. B. K. Minhas, S. A. Coulombe, S. S. H. Naqvi, and J. R. McNeil, "Ellipsometric scatterometry for the metrology of sub-0.1-μ-linewidth structures," *Appl. Opt.* **37**(22), 5112–5115 (1998).
14. H. Huang and F. L. Terry, Jr., "Spectroscopic ellipsometry and reflectometry from gratings (scatterometry) for critical dimension measurement and *in situ*, real-time process monitoring," *Thin Solid Films* **455–456**, 828–836 (2004).
15. S. A. Coulombe, B. K. Minhas, and C. J. Raymond, "Scatterometry measurement of sub-0.1-μ linewidth gratings," *J. Vac. Sci. Technol. B* **16**(1), 80–87 (1998).
16. E. M. Drege and D. M. Byrne, "Lithographic process monitoring using diffraction measurements," *Proc. SPIE* **3998**, 147–157 (2000).
17. R. M. Al-Assaad and D. M. Byrne, "Error analysis in inverse scatterometry," *J. Opt. Soc. Am. A* **24**(2), 326–338 (2007).
18. H. D. Rowland, W. P. King, A. C. Sun, and P. R. Schunk, "Simulations of nonuniform embossing: the effect of asymmetric neighbor cavities on polymer flow during nanoimprint lithography," *J. Vac. Sci. Technol. B* **23**(6), 2958–2962 (2005).

Rayan M. Al-Assaad received a BS degree in computer science from the Lebanese American University, Lebanon, in 1998, and MS and PhD degrees in electrical engineering from the University of Texas at Dallas, Richardson, in 2003 and 2006, respectively. He is currently working as a postdoctoral research associate with the Department of Electrical Engineering at the Eric Jonsson School of Engineering and Computer Science at the University of Texas at Dallas, Richardson. His research interests are optical metrology and nanophotonics. He is currently working on scatterometry for nanolithography applications. He is an active member of OSA and SPIE and a reviewer in applied optics.

Li Tao received his BS degree (with honors) in materials science and engineering from Southeast University, Nanjing, China, in 2004 and then worked as a research assistant on a Chinese national 863 funded project. Since 2006, he has been a graduate student and research assistant in the Department of Electrical Engineering of the University of Texas at Dallas, Richardson. His research interests include electron beam lithography, nanoimprint lithography, nanocharacterization, and biomedical nano devices. He has been a student member of IEEE and the Material Research Society (MRS) since 2006.

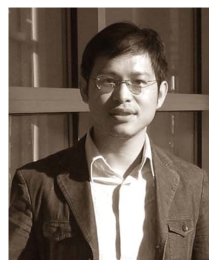

Wenchuang Hu received a BS degree from Peking University, Beijing, China, in 1999, and MSEE and PhD degrees from the University of Notre Dame, Indiana, in 2001 and 2004, respectively. He spent a year as a postdoctoral research fellow at the Solid State Electronics Laboratory, Department of Electrical Engineering and Computer Science, University of Michigan, Ann Arbor. In 2005, he joined the Department of Electrical Engineering of the University of Texas at Dallas as an assistant professor. His research interests include engineering nanostructured biomaterials, metrology for polymer nanostructures, and fabrication of electrical and optical nano devices using a combination of nanolithography and self-assembly. His expertise is in the areas of electron beam lithography, nanoimprint lithography, and nanofabrication processes and metrology. He is familiar with surface chemistry, polymer science, and cell biology. He is an active member of Sigma Xi, IEEE, MRS, SPIE, and AVS. He serves as a journal reviewer for *Nanotechnology, IEEE Transactions on Nanotechnology, Journal of Vacuum Science and Technology, Surface and Coating Technology, Microelectronic Engineering*, and *Applied Physics Letters*. He also serves as a panelist for the National Science Foundation.